Sedimentary Geology 343 (2016) 132–140

Contents lists available at ScienceDirect

Sedimentary Geology

journal homepage: www.elsevier.com/locate/sedgeo

Abiotically-formed, primary dolomite in the mid-Eocene lacustrine succession at Gebel El-Goza El-Hamra, NE Egypt: An approach to the role of smectitic clays

H.A. Wanas [a,*], E. Sallam [b]

[a] Department of Geology, Faculty of Science, Menoufiya University, Shebin El-Kom, Egypt
[b] Department of Geology, Faculty of Science, Benha University, Benha, Egypt

ARTICLE INFO

Article history:
Received 4 July 2016
Received in revised form 8 August 2016
Accepted 9 August 2016
Available online 18 August 2016

Editor: Dr. J. Knight

Keywords:
Abiotic
Primary dolomite
Smectitic clays
Lacustrine
Mid-Eocene
Egypt

ABSTRACT

This study discusses the role of smectitic clays in the formation of an abiotic (physio-chemical) primary dolomite within an evaporative alkaline-saline marginal lake system, in the absence of carbonate precursor and microbes. The present work has been achieved in terms of textural, mineralogical, and geochemical characteristics of dolostones in the Mid-Eocene (Bartonian) lacustrine succession cropping out at Gebel El-Goza El-Hamra (Shabrawet area, NE Egypt). This lacustrine succession is 15–16 m thick, and made up of alternating horizontal beds of dolostone, marlstone and mudrock that show some pedogenic and subaerial exposure features. The dolostones are composed mainly of dolomite (60–90%), smectite (20–30%) and quartz grains (5–10%). The dolomite comprises fine-crystalline rhombs to micro-spherical crystals with no obvious relics of microbial activity and/or carbonate precursor. It is, ordered, nearly stoichiometric (with 46–50% mole of $MgCO_3$) and has $\delta^{18}O$ and $\delta^{13}C$ values ranging from +0.44 to +2.96 VPDB ‰, and 0.93 to −8.95 VPDB ‰, respectively. The smectite occurs as thin mats that are commonly intergrown and associated with dolomite. Mineralogical, textural and stable isotopic results of the dolomite indicated that the dolomite was formed as an abiotic primary precipitate in alkaline saline lacustrine systems. In this respect, the gel-like highly viscous smectitic medium plus progressive CO_2 degassing, elevated evaporation, low sedimentation rate, low sulphates level and alkaline soil solution lowered the kinetic barriers of dolomite precipitation from solution and promoted the incorporation of Mg^{2+} in the structure of dolomite. Consequently, the presence of smectitic clays in evaporative saline lakes is significant for dolomite formation because they can generate a gel-like highly viscous medium and provide Mg^{2+} that can facilitate the physcio-chemical precipitation of primary dolomite from solution at ambient temperatures. However, more work is needed to better characterize the role of clays during dolomite formation in alkaline lacustrine environments at ambient temperatures.

1. Introduction

In lacustrine/palustrine environments, dolomite can form by microbial activities (e.g., Last, 1990; Vasconcelos et al., 1995; Vasconcelos and McKenzie, 1997; Wright, 1999; García del Cura et al., 2001; Calvo et al., 2003; Wright and Wacey, 2005; Wacey et al., 2007; Sánchez-Román et al., 2008; Bréhéret et al., 2008; Deng et al., 2010; Casado et al., 2014) and/or by the dolomitization of carbonate muds precursor (e.g., Last, 1990; Arenas et al., 1999; Bustillo et al., 2002; Yuan et al., 2015). In contrast, the abiotic formation of lacustrine/palustrine dolomites from solution in ambient and inorganic (physio-chemical) conditions with no microbial mediation and carbonate mineral precursors is more rarely recognized and still requires more attention (De Deckker and Last, 1989; Botha and Hughes, 1992; Wanas, 2002; Bristow et al., 2012; Zhang et al., 2012; Roberts et al., 2013; Casado et al., 2014; Wright and Barnett, 2015). Additionally, a close relationship between abiotic dolomite formation and clays has been previously documented in caves (Polyak and Güven, 2000; Martín Pérez et al., 2015) and soils (Díaz-Hernández et al., 2013; Casado et al., 2014; Koster and Gilg, 2015; Cuadros et al., 2016). On the other hand, no previous studies have been undertaken on the role of smectitic clays in the enhancement of abiotic primary dolomite formation in lacustrine/palustrine systems, except the work of Botha and Hughes (1992) who suggested that neoformed (non-replacive) abiotic dolomite can form in marginal lacustrine sediments by the action of alkaline soil solutions, including decomposition products released during breakdown of smectite and palygorskite. Therefore, the present study can give an insight on the mechanism of formation of lacustrine abiotic dolomite with the aid of smectitic clays in the absence of microbial activities and carbonate precursors. To achieve this, detailed mineralogical, textural and stable isotopic studies of the mid-Eocene (Bartonian) lacustrine dolomites at Gebel El-Goza El-Hamra (NE Eastern Desert, Egypt) have been carried out.

* Corresponding author at: Geology Department, Faculty of Sciences, Menoufiya University, Shebin El-Kom, Egypt.
E-mail addresses: hamdallahwanas@yahoo.com (H.A. Wanas), emad.salam@fsc.bu.edu.eg (E. Sallam).

http://dx.doi.org/10.1016/j.sedgeo.2016.08.003
0037-0738/

2. Geological setting and lithostratigraphy

Gebel El-Goza El-Hamra is located at the Shabrawet area, NE Eastern Desert, Egypt (Fig. 1). The Shabrawet area was subjected to orogenic movements (i.e., the Syrian Arc System), which started in the late Cretaceous and continued intermittently until the late Miocene (Al-Ahwani, 1982; Moustafa and Khalil, 1995; Haggag, 2010). The Shabrawet area includes two major NE–SW asymmetrical anticlines enclosing a shallow syncline (Al-Ahwani, 1982). The cores of the Shabrawet anticlines are mainly represented by Cretaceous rocks. On the southern flanks of these anticlines, the Cretaceous rocks are unconformably overlain by sub-horizontal Eocene rocks that are then covered by Oligocene sand and gravels. On their northern flanks, the Cretaceous rocks are mainly covered by horizontal to sub-horizontal Oligocene and Miocene strata (Al-Ahwani, 1982; Said, 1990; Haggag, 2010) (Fig. 1). Generally, the Eocene, Oligocene and Miocene rocks constitute several dissected scarps around the Shabrawet anticlines. Numerous faults trending ENE and NW–SE dissect the Shabrawet area. The older ENE faults affected the Cretaceous rocks in both anticlines, prior to the deposition of the Eocene sediments (Al-Ahwani, 1982). Along the NW–SE trending faults (Clysmic or Erythrean), many of the Eocene scarps have developed in the Shabrawet area.

Lithostratigraphically, the Shabrawet area is covered by a thick sedimentary succession that ranges in age from early Cretaceous to Neogene (Al-Ahwani, 1982; Said, 1990). The Eocene rocks occur as horizontal to sub-horizontal beds, and have an unconformable relationship with their underlying highly deformed Cretaceous strata (Al-Ahwani, 1982). They are disconformably overlain by Oligocene and/or Miocene rocks (Al-Ahwani, 1982). At Gebel-El-Goza El-Hamra, the Eocene succession has been subdivided into three lithostratigraphic units (Sallam et al., 2015) that are, from base to top: the Minia Formation (late Ypresian), the Sannor Formation (Bartonian), and the Maadi Formation (Priabonian). These three formations are disconformable with each other (Sallam et al., 2015). On the basis of its lithological characteristics, the mid-Eocene (Bartonian) Sannor Formation at GebelEl-Goza El-Hamra has been subdivided by Sallam et al. (2015) into three informal rock units: lower (Sn-1), middle (Sn-2) and upper (Sn-3) units. In this study, we agree with and follow the mid-Eocene lithostratigraphic subdivision of Sallam et al. (2015). The studied succession constitutes the uppermost part of the Sn-2. It is also equivalent to the uppermost part of the mid-Eocene El-Goza El-Hamra Formation of Hassan and Omran (1991) and clastic wedge unit of Selim et al. (2016).

3. Materials and analytical methods

This study is based on data gathered during detailed fieldwork at Gebel El-Goza El-Hamra (Shabrawet area, NE Eastern Desert, Egypt) complemented by laboratory analyses. Forty-two samples of dolostones and mudrocks were collected from two outcrops for the uppermost part of the middle unit (Sn-2) of the Sannor Formation at Gebel El-Goza El-Hamra (see Fig. 1 for locations). For optical petrographic study, thirty-five standard thin sections of consolidated dolomite samples were prepared following the method of Keyes (1925) and then photographed using an Olympus BX51 polarizing light microscope equipped with an integrated Olympus LC20 digital built-in-camera. Dolomite textures are described following the classification of Sibley and Gregg (1987). The bulk-rock mineralogy of selected samples was analyzed using a Philips PW-1752 X-ray diffraction (XRD) system, operating at 40 kV and 30 mA, with Ni filter and Cu-Kα radiation ($\lambda = 1.54060$ Å). XRD analysis was performed following the method of Chung (1974) using EVA Bruker software. The percentage mole value of $MgCO_3$ was determined following Goldsmith et al. (1961). The degree of ordering of dolomite was determined from diffraction peaks, with correlation between intensity of (015) and (110) peaks

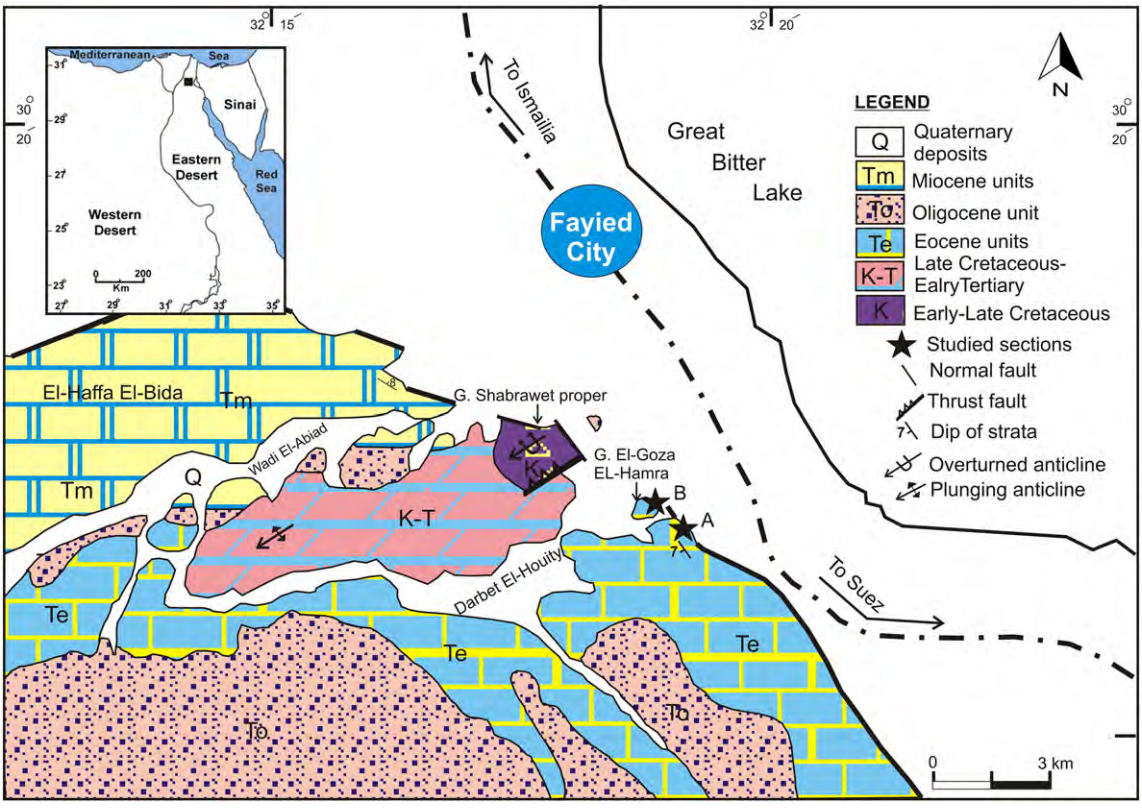

Fig. 1. Geological map of the studied area in Shabrawet (NE Eastern Desert, Egypt), modified after (Al-Ahwani, 1982).

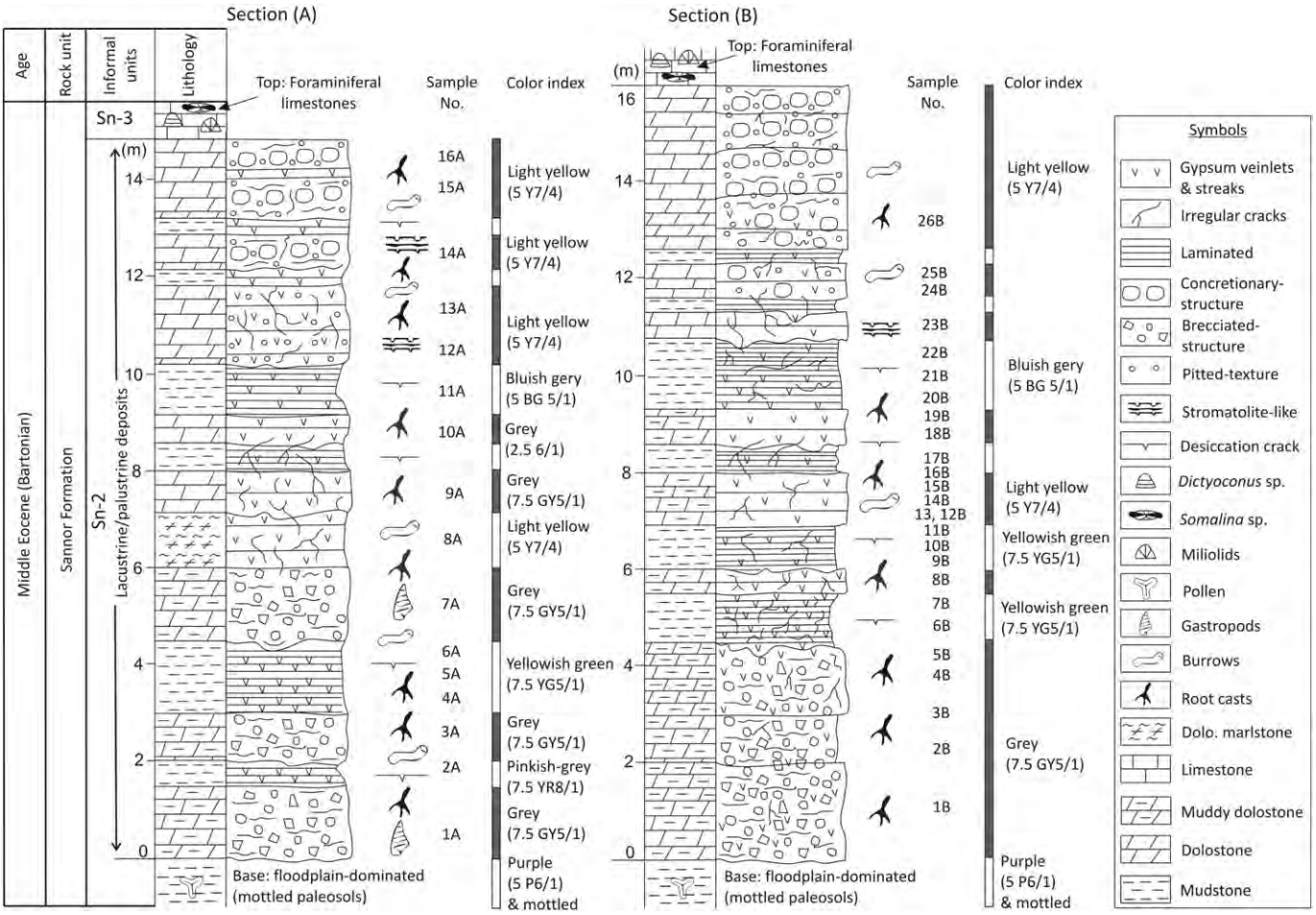

Fig. 2. Lithostratigraphic column sections (A and B) of the lacustrine succession at Gebel El-Goza El-Hamra, NE Eastern Desert, Egypt. Sn-2 and Sn-3 refer to the middle unit and upper unit of the Sannor Formation, respectively.

measured according to standard procedures (Hardy and Tucker, 1988). Identification and estimate of the clay mineralogy in the clay-rich samples was carried out on oriented aggregate samples (for fractions <2 μm) using air-dried, glycolated and thermal treated mounts (Brindley, 1980). The ethylene glycolated oriented mounts were kept in ethylene vapor heated at 60 °C for 24 h whereas the thermal treated mounts where heated for 550 °C for 3 h. Quantitative mineralogy was determined from XRD patterns of whole-rock powders spiked with 11.1 wt% zinc oxide using Rockjock-program that runs in Microsoft Excel (Eberl, 2003).

Back scattered images (BSE) and electron microprobe analysis (EMPA) for dolostone samples were carried out on carbon-coated polished thin sections using a JEOL Superprobe JXA 8900-M wavelength dispersive electron microprobe analyzer (WDS-EMPA) equipped with four crystal spectrometers and beam diameter between 2 and 5 μm to minimize damage from the electron beam. Scanning electron microscopic (SEM) observations were carried out on gold-coated samples, to obtain high-resolution textural and morphometric images. Fresh pieces were placed on sample holders supported by carbon conductive tape, followed by sputter coating of gold and then investigated using a JEOL JSM-820 microscope working at 20 kV, and equipped with an energy dispersive X-ray microanalyzer (EDX).

Carbon ($\delta^{13}C$) and oxygen ($\delta^{18}O$) isotopic analyses were determined for micro-drilled dolomite powder samples following the methods of McCrea (1950) and Spötl and Vennemann (2003). For these analyses, small amounts (0.5–1.0 mg) of powders were dried and placed in an oven at 70 °C for 10 h before being moved to the instrument. Carbon dioxide was released using 100% phosphoric acid at 70 °C and analyzed on-line in a DELTA plus XP + Gas Bench mass spectrometer. Carbon and oxygen isotopic compositions for dolomite were reported using standard δ notation in units of ‰ relative to V-PDB standard (the Vienna Pee Dee Belemnite standard) where two values of the measurements were reported.

4. Sedimentology of the mid-Eocene rocks

At Gebel-El-Goza El-Hamra, the mid-Eocene rocks belong to the Sannor Formation that was subdivided by Sallam et al. (2016) into three informal rock units : lower (Sn-1), middle (Sn-2) and upper (Sn-3) units. The Sn-1 is composed of about 20 m thick of brownish green claystones interbedded with foraminiferal limestones (rich in *Dictyoconus aegyptiensis* and *Idalina cuvillieri*) and highly dissected by gypsum streaks. The Sn-2 (in which the studied strata are developed) is 45 m thick and consists of claystone, siltstone and coarse-grained sandstone with conglomerate lens that topped by about 15 m thick of thin-bedded dolostones, marlstones and mudrocks. The Sn-3 is 20 m thick and is composed of bryozoan/foraminiferal limestones rich in *Somalina stefaninii*. These different mid-Eocene rock units were considered as deposits of shallow marine environments (Al-Ahwani, 1982; Abu El-Ghar, 2007; Hassan and Omran, 1991). On the other hand, Sallam et al. (2015) and Wanas et al. (2015) declared that these mid-Eocene deposits were developed in different depositional environments. They suggested that the rocks of the Sn-1 and Sn-3 were deposited in a marginal marine (tidal flat to lagoonal) environment on an inner ramp platform, whereas the Sn-2 was considered as deposits of floodplain-dominated

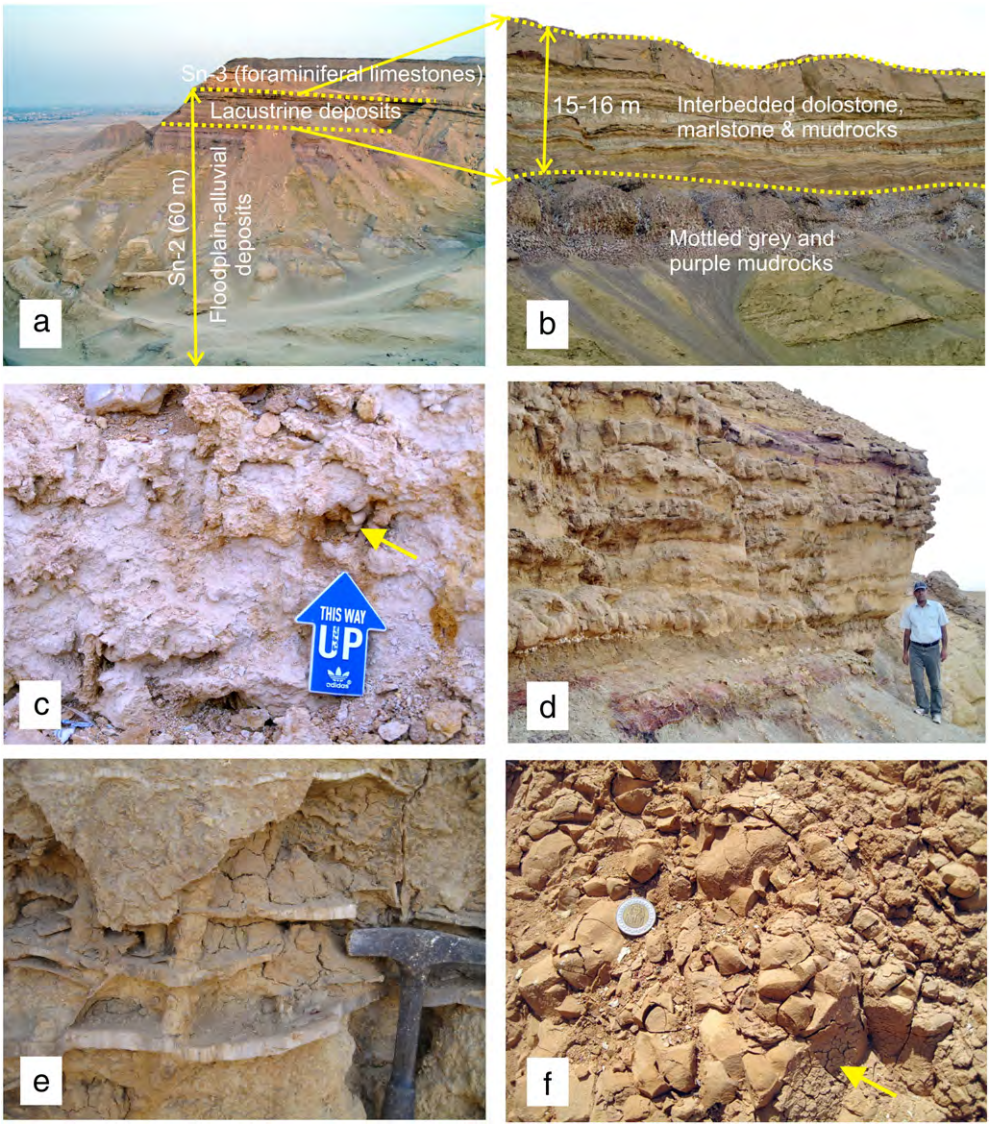

Fig. 3. Field photos showing: (a) the stratigraphic position of the studied lacustrine deposits at Gebel El-Goza El-Hamra, (b) a close-up of dolostones and mudrocks of the studied lacustrine succession overlying the mottled mudrocks of the floodplain-dominated succession, (c) small gastropod cast (arrow) embedded in the studied deposits, (d) the studied succession that consists of greenish yellow mudrock, yellow marlstone and reddish yellow dolostone beds. The mudrock and marlstone beds form gullies in-between dolostone ledges. Notice, the irregularly beddings and concretionary-like structures in the dolostone beds. Person for scale is 1.65 m, (e) root casts and gypsum veins dissect the mudrocks and dolostone deposits, hammer handle for scale is 26 cm long, (f) nodular-brecciated structure of dolostone, embedded in an argillaceous matrix (arrow), coin for scale is 2.4 cm in diameter.

alluvial-lacustrine systems, under arid and semiarid climatic conditions. Recently, Selim et al. (2016) showed that the mid-Eocene rocks were deposited in environments vary from a stream-dominated delta to lagoonal deposits through the delta fringes. However, they did not notice the occurrence of about 15–16 m thick shallow lacustrine deposits that directly occur below the lagoonal foraminiferal limestones of Sn-3, and unconformably overlie the alluvial-floodplain siliciclastic deposits of Sn-2. The present study is concerned with the lacustrine succession that forms the uppermost part of the mid-Eocene Sn-2 of Sallam et al. (2015).

5. Field and facies description of the studied succession

5.1. Outcrop features

The study outcrop occurs as gently sloped small hills separated by small incised water gullies. The studied succession constitutes the uppermost part of the Sn-2 (Fig. 2). It unconformably overlies the alluvial floodplain siliciclastic deposits (25 m thick) of the Sn-2 (Fig. 3a, b), and underlies the marginal marine deposits of the Sn-3 (Fig. 2). It consists mainly of mixed siliciclastic-carbonate rocks (15–16 m thick) (Figs. 2), without marine fossils, except the rarely occurrence of small gastropod casts (Fig. 3c). This succession is made up of alternated beds of dolostone, marlstone and mudrock with a few thin layers of siltstone (Figs. 2, 3d).

5.2. Facies description

5.2.1. Dolostone facies

The dolostone beds are irregularly bedded and display concretionary-like structures (Fig. 3d). Their contacts are sharp with the underlying and overlying mudrock facies. Thickness of the dolostone beds ranges from 0.3 to 0.7 m, and they largely increase in thickness towards the top of the succession (Fig. 2). The dolostones are yellow to reddish yellow in color and hard. Such reddish coloration of dolostones is due to their contamination with iron minerals. In the uppermost part of the succession, the dolostones display some karst-features (cavernous-like). Some paleopedogenic and subaerial exposure features were observed in the dolostone beds. These features comprise root casts, color mottling, gypsum veins and nodular-brecciated structures (Fig. 3e, f).

Table 1
Mineralogical and stable isotopic results of the dolostone samples. Dol = Dolomite; Qz = Quartz; Cl = Clay.

Sample no.	% Mineralogy (semi-quantitative)			Isotopes (‰ VPDB)	
	Dol.	Qz.	Cl.	$\delta^{18}C$	$\delta^{13}O$
1A	70	8	22	−7.16	+1.59
3A	30	30	40	−5.46	−1.08
10A	90	10	–	−3.92	−1.61
13A	30	30	40	−4.18	+1.12
16A	85	5	10	+0.27	+0.90
5B	25	40	35	−7.07	+1.26
8B	75	–	25	−8.95	−2.96
11B	60	5	35	−5.32	+0.44
18B	55	15	30	−4.63	+1.84
28B	60	15	25	−0.93	+0.81

5.2.2. Mudrock and marlstone facies

The mudrocks and marlstones occur as alternating beds with the dolostones (Fig. 3d). They show gradual contacts with the dolostones and marlstones (Fig. 3d). The mudrock beds range in thickness from 10 to 50 cm (Fig. 2). Two types of mudrock facies have been recognized: (1) yellowish green, massive with a soapy appearance mudrocks, and (2) pink to purple, massive with conchoidally structure mudrocks. Mudrocks show irregular mm-wide desiccation cracks partially filled with white gypsum. The marlstones are yellow in color, massive and each bed of them reaches up to 60 cm thick (Fig. 2).

6. Results

6.1. Mineralogy and petrography of dolostones

Semi-quantitative XRD showed that the main minerals in the dolostone facies are dolomite (60–90%), clays (20–30%) and quartz grains (5–10%) (Table 1). Calcite or other carbonate and evaporite minerals have not been detected. In addition to examination of dolostone facies, we investigate the mudrock facies that occurs between dolostone facies. Mineralogically, the mudrock facies is composed of clay minerals (40%), quartz (30%) and dolomite (30%) (Table 1). In thin section, dolomite occurs as fine-crystalline rhombs (20–30 μm in size) that display hypidiotopic fabric and equigranular texture (Fig. 4a). These rhombs are not well-zoned but have cloudy cores due to the presence of very fine opaque dusty inclusions (Fig. 4a). Fine-crystalline spherical dolomite (rounded to subrounded) crystals were also noted (Fig. 4b). Clay matrix occurs as thin mats between the dolomite rhombs (Fig. 4a, b), and its identification by bulk XRD was difficult. Under SEM, the clay mats form irregular curved flakes in between and surrounding the dolomite rhombs (Fig. 4c, d). Also, they intergrow with the dolomite rhombs (Fig. 4e, f), and display honeycomb structures enclosed within dolomite rhombs (Fig. 4g, h). Based on their morphology (Fig. 4c–h), clay mats can be interpreted as smectite. Also, as revealed from probe chemical analysis (EPMA, Table 2), clay matrix correspond with a composition broadly similar to Mg-smectite?. In this respect, the increase of Fe percentage in the smectitic clay matrix (Table 2) could be resulted from their contamination with iron minerals (as indicated by reddish yellow color of dolostones and mudrocks, Fig. 3c). In both thin sections and SEM examination, no microbial evidence (e.g., dolomicrite filaments, peloids, and alveolar septal fabric, root cells, spherulites, micro-rods, nano-spheres calcified microbial coatings and *Microcodium*, see Wright, 1999) has been observed in the studied dolomites.

6.2. Stoichiometry and stable isotopes of dolomite

The percentage mole value of $MgCO_3$ was determined by the correlation with the (104) peak reflection of dolomite, following Goldsmith et al. (1961). The degree of ordering of dolomite was determined from diffraction peaks according to standard procedures (Hardy and Tucker, 1988). X-ray diffraction analysis demonstrates that the studied dolomite is ordered and nearly stoichiometric as indicated by the (104) peak reflection at values between 30.88° and 31.04° (Fig. 5) that reflect the excess of mole% $MgCO_3$ (between 46% and 50% mole, respectively) in the structure of the dolomite (Morse and Mackenzie, 1990). $\delta^{18}O$ values of the studied dolostones range between +0.44 and +2.96 VPDB‰, whereas their $\delta^{13}C$ values range between −0.93 and −8.95 VPDB ‰ (Table 1). Three dolomite samples show slightly negative $\delta^{18}O$ values (−1.08 ‰ to −2.96‰) (Table 1). The stable isotopic compositions of the studied dolostone samples do not show any covariant trend between $\delta^{13}C$ and $\delta^{18}O$ values (Fig. 6).

7. Discussion

In lacustrine/palustrine environments, several processes had been considered to interpret the primary/diagenetic dolomite. The first is the fact that the dolomicrite can precipitate by microbial activity where microbes modify the chemistry of the solution, and provide suitable surfaces for nucleation of a poorly-ordered, fine-crystalline, Ca-rich dolomite (e.g., Vasconcelos et al., 1995; Wright, 1999; García del Cura et al., 2001; Van Lith et al., 2003; Wacey et al., 2007; Bréhéret et al., 2008; Sánchez-Román et al., 2008; Deng et al., 2010; Last et al., 2012). The second is that the dolomicrite can form by dolomitization of carbonate muds precursors (e.g., Last, 1990; Arenas et al., 1999; Bustillo et al., 2002; Yuan et al., 2015). In the studied dolostones, there is any evidence for carbonate precursors and microbial activity. Therefore, the studied dolomite appears to be a primary precipitate due to its occurrence as homogeneous-sized dolomicrite (see Fig. 4a, b), and lack of any preserved other carbonate minerals precursor (De Deckker and Last, 1989; Last, 1990; Arenas et al., 1997; El-Sayed, 2001; García del Cura et al., 2001; Abdul Aziz et al., 2003; Bréhéret et al., 2008). Also, this dolomite seems to be abiogenically-formed, as indicated by the absence of any microbial relics (see Section 6.1) within the studied dolomites. The recorded positive $\delta^{18}O$ signature (+0.44 and +2.96 VPDB‰) indicates that dolomite precipitation was probably mediated by evaporative alkaline-saline lake conditions (Bellanca et al., 1992; Calvo et al., 1995; Abdul Aziz et al., 2003; Arenas et al., 1997; Mauger and Compton, 2011; Yuan et al., 2015) and low temperatures, as all values of oxygen isotopes (Table 1) are larger than the limit value (−6.5‰) for high-temperature dolomite genesis (Allan and Wiggins, 2003; Yuan et al., 2015). The slightly negative $\delta^{18}O$ values (−1.08 ‰ to −2.96‰) of the dolomites may be due to the overlapping of pedogenesis and meteoric diagenesis (Bustillo and Alonso-Zarza, 2007; Armenteros and Edwards, 2012; Li et al., 2013). On the other hand, the recorded negative $\delta^{13}C$ values (−0.93 and −8.95 VPDB ‰) indicate that precipitation of dolomites is more likely to have taken place through the degradation of organic matter (Calvo et al., 1995; Mauger and Compton, 2011; Armenteros and Edwards, 2012). It also indicates soil-derived CO_2 from root respiration under semi-arid climatic conditions (Li et al., 2013) which may also promote negative $\delta^{13}C$ values of the lake water (Armenteros and Edwards, 2012; Li et al., 2013). Additionally, the recorded negative $\delta^{13}C$ values of the studied dolomites do not show the characteristic wide range of $\delta^{13}C$ values often associated with 'organogenic' or bacterially-induced carbonates and dolomites (e.g., Warren, 2000; García del Cura et al., 2001; Leveille et al., 2007; Wacey et al., 2007; Solari et al., 2010).

Textural and mineralogical characters of the studied dolomite (see Section 6.1) reveal its occurrence in close association with a clayey material that is composed mainly of smectites. Such characteristics suggest a genetic relationship between dolomite and smectite rather than a simple juxtaposition of the two minerals. Therefore, dolomite formation needs now to connect with the presence of smectite minerals in the precipitation medium. As revealed from petrographic characters of dolomite with its associated smectite (Fig. 4a–h), the studied dolomite has been interpreted as

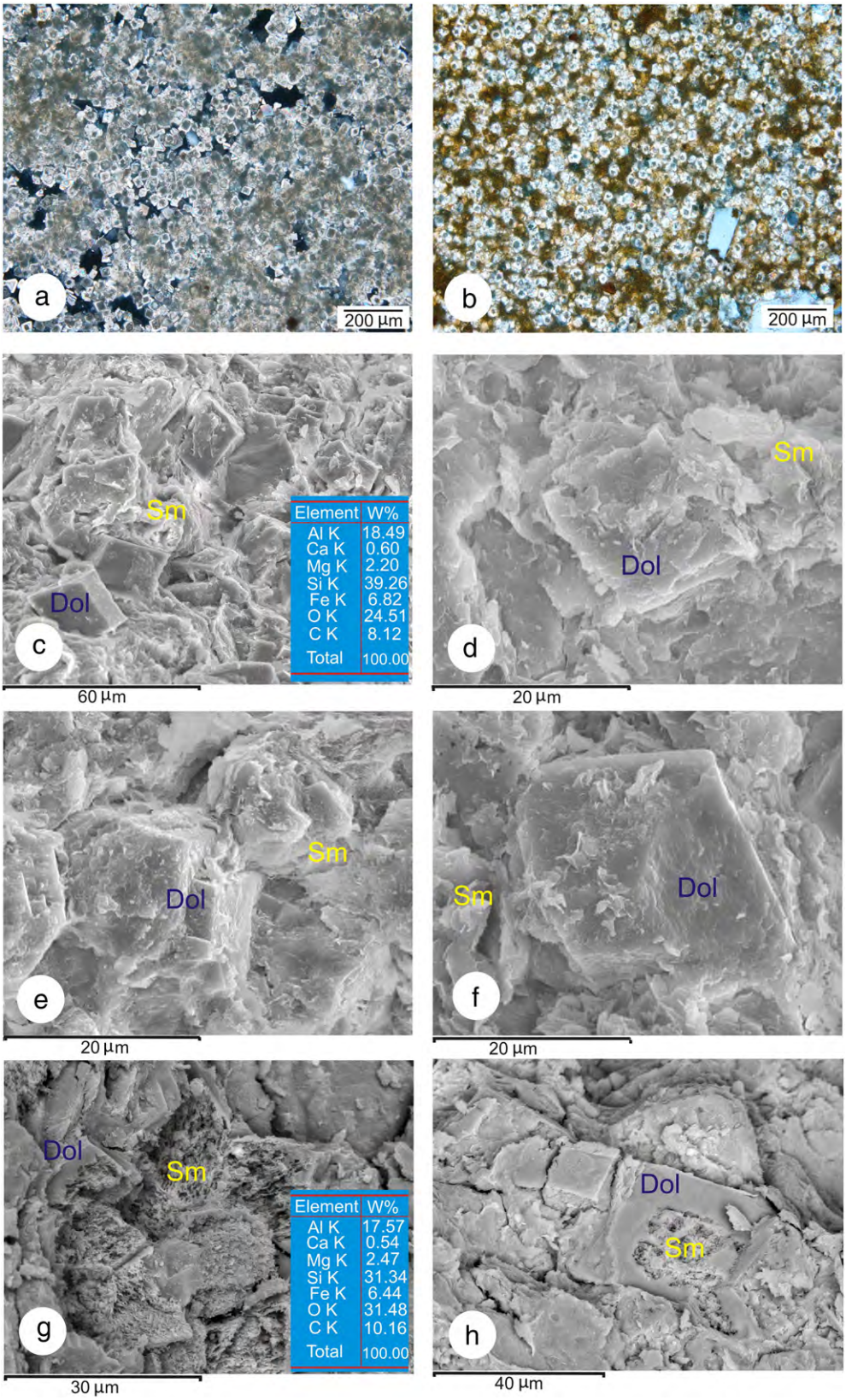

Fig. 4. (a, b) Photomicrographs showing fine-crystalline dolomite rhombs with hypidiotopic fabric and equigranular texture (right-hand photo). Notice the occurrence of some anhedral, micro-spheroidal crystals (left-hand photo), samples no. 1 A and 10 A, respectively, (c) SEM image showing dolomite rhombs surrounded by irregular curved flakes-smectite, sample no. 25B, (d–F) SEM images showing intergrowth of curved flakes-smectite with dolomite rhombs, samples no. 2B and 8B, respectively, (g, h) SEM images showing honeycomb-like structure-smectite enclosed in the dolomite rhombs, samples no. 2B and 13A. Dol = Dolomite; Sm = Smectite. EDX elemental analyses on the Fig. 4c, g refer to smectitic clays (Sm).

Table 2
Electron microprobe analyses (EMPA) for the dolomite crystals and their associated clay matrix in the studied dolostones. All data are expressed in percentage (%).

Sample no.	Spot location	Al_2O_3	FeO	K_2O	CaO	MgO	SrO	MnO	BaO	P_2O_5	Na_2O	SiO_2	Total (%)
13	Dolomite	0.151	0.816	0.005	31.508	19.594	0.063	0.116	0.018	0.105	0.063	–	52.439
	Dolomite	0.070	1.116	0.012	30.777	20.050	0.047	–	0.066	0.102	0.082	–	52.322
	Clay matrix	22.973	7.558	1.777	0.600	2.045	–	0.014	0.008	0.050	0.184	49.207	84.416
	Dolomite	0.480	1.202	0.043	30.104	19.355	0.077	0.320	–	0.127	0.019	0.397	52.124
	Clay matrix	23.494	6.825	2.558	0.606	2.196	–	–	0.121	0.081	0.263	42.585	78.729
16A	Dolomite	0.063	0.292	0.007	32.702	18.580	0.181	0.199	0.016	0.049	0.043	–	52.132
	Dolomite	0.139	0.567	0.016	31.561	18.807	0.175	0.192	–	0.034	0.051	–	51.542
	Clay Matrix	20.579	16.602	1.600	0.536	2.468	–	–	0.048	0.198	0.153	36.336	78.520
	Dolomite	0.017	0.088	0.017	34.900	18.447	0.162	–	–	0.065	0.124	–	53.820
2B	Clay matrix	18.440	8.656	1.448	0.438	2.414	–	0.013	0.053	0.027	0.063	33.700	65.252
	Clay matrix	13.498	36.940	0.508	1.155	2.421	–	0.081	–	0.052	0.124	18.882	73.661
	Dolomite	0.238	0.731	0.015	32.353	19.298	0.045	00.205	0.161	0.098	0.118	–	53.262
	Dolomite	0.695	0.407	0.014	32.594	19.512	0.170	0.099	0.020	0.028	0.059	–	53.598
	Dolomite	0.127	1.820	0.037	31.121	18.715	0.085	0.383	0.032	0.029	0.093	0.090	52.532
	Clay matrix	25.081	9.680	1.806	0.428	3.137	–	0.097	0.075	0.094	0.058	45.339	85.795
15B	Dolomite	0.726	1.818	0.089	29.696	19.458	0.012	0.172	–	0.074	0.046	0.984	53.075
	Dolomite	0.500	1.805	0.047	29.521	18.672	0.070	0.125	–	0.065	0.076	0.543	51.424
	Dolomite	0.361	1.898	0.088	30.157	18.970	–	0.238	0.060	0.100	0.080	0.361	52.313

a primary precipitate enclosing the previously-precipitated smectitic clay minerals. This can be discussed in the following:

From the textural, mineralogical and stable isotopic analyses, the studied dolomite appears to be a primary precipitate in origin (rather than replacement of precursor carbonate minerals), and was precipitated in evaporative alkaline-saline lake water with low sulphate concentration under semi-arid conditions and low temperatures. In such conditions, smectite could form by direct precipitation from solution in alkaline-saline lake, where the alkaline-saline waters containing silica, Fe and Al-rich detrital clays (kaolinite, which is unstable in alkaline lacustrine conditions and provides Al to solution; Chahi et al., 1993) promoted the precipitation of authigenic smectite (Jones, 1986; Darragi and Tardy, 1987; Calvo et al., 1999; Polyak and Güven, 2000; Deocampo, 2005, 2015; Furquim et al., 2008; Bristow and Milliken, 2011; Martín Pérez et al., 2015; Gürel and Özcan, 2016). In such high pH (over 9) environments, smectitic clays may be neoformed as a gel-like highly viscous medium (Pozo and Casas, 1999; Tosca and Masterson, 2014; Cuadros et al., 2016; Díaz-Hernández et al., 2013; Casado et al., 2014; Wright and Barnett, 2015). By increase evaporation (as indicated by positive oxygen isotope values), such a highly viscous smectitic alkaline medium with low sulphate concentrations (as is evidenced by the absence of any associated sulphate minerals) could clearly lower kinetic barriers for abiotic formation of primary dolomite enclosing the previously-precipitated smectitic clay minerals (Fernández-Díaz et al., 2006; Sánchez-Navas et al., 2009; Díaz-Hernández et al., 2013; Casado et al., 2014; Wright and Barnett, 2015; Cuadros et al., 2016). In such conditions and settings, the Ca, Mg and HCO_3 for dolomite formation were probably came to the studied mid-Eocene lake water from: 1) high evaporation in the saline lake water, where high evaporation rates can produce pore waters with sufficiently high Mg/Ca ratios and carbonate ion concentrations to precipitate dolomite (Last, 1990; Calvo et al., 1999), 2) the presence of smectite which can act as a catalyst for incorporation of Mg^{+2} in the carbonates phases, and/or as templates for direct precipitation of dolomite (Díaz-Hernández et al., 2013; Casado et al., 2014; Martín Pérez et al., 2015; Wright and Barnett, 2015; Mercedes-Martin et al., 2016), 3) a percolation of alkaline soil solutions during pedogenesis that favour the incorporation of Mg^{+2} into the dolomite structure (Botha and Hughes, 1992; Whipkey et al., 2002; Whipkey and Hayob, 2008;

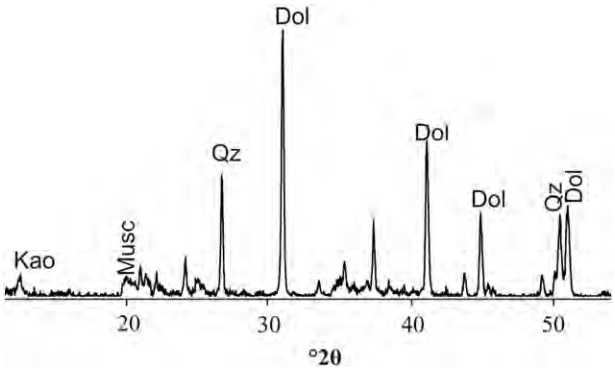

Fig. 5. X-ray powder diffraction pattern of the encountered minerals in the studied dolostone. Dol = Dolomite; Qz = Quartz; Kao = kaolinite and Musc = Muscovite.

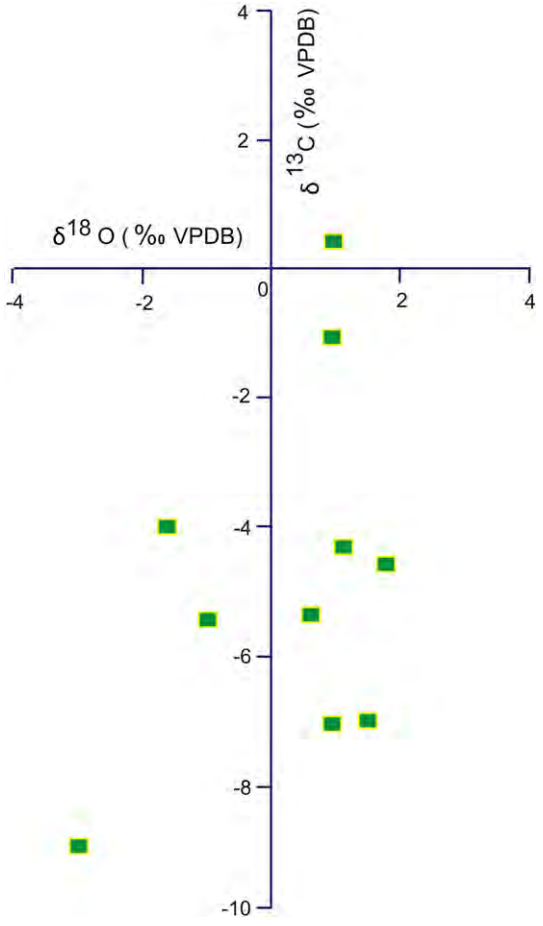

Fig. 6. $\delta^{18}O$ and $\delta^{13}C$ cross plots for the dolomite samples.

Casado et al., 2014; Alonso-Zarza et al., 2016), 4) the decomposition of soil organic matter (see negative $\delta^{13}C$ values) that increases the alkalinity and Mg/Ca ratio in the lake water (Talbot, 1990), 5) dissolution of dolostone and limestone clasts that were derived from the surrounding Cretaceous strata, and 6) aeolian dusts that reflect aridity to semi-aridity in the mid-Eocene at the studied area (Wanas et al., 2015).

8. Conclusions

In some saline and alkaline lake systems, smectitic clay minerals forming at or near the sediment water interface are a major sedimentary component. These clays influence the physical and geochemical budget of lake waters, and are therefore expected to influence the formation of contemporaneous carbonate precipitates. Also, dolomite may occur relatively commonly as the only carbonate mineral if the sedimentary, soil or diagenetic solutions are alkaline. The studied mid-Eocene lacustrine succession at Gebel El-Goza-El-Hamra (Shabrawet area, NE Egypt) gives us an opportunity to study a systematic feedback between smectitic clays and direct dolomite formation in alkaline lake systems under arid to semiarid climates at ambient temperatures. In the studied section, smectitic clays and fine-crystalline dolomites were formed in an evaporative alkaline lacustrine environment at ambient (low) temperatures in the absence of both microbial activities and carbonate precursors. In such conditions, smectitic clays were neoformed as a gel-like highly viscous materials. Elevated evaporation in such highly viscous smectitic alkaline medium that has low sulphate concentrations and alkaline soil solution supply clearly lower kinetic barriers for abiotic dolomite formation as a primary precipitate. Consequently, neoformation of smectitic clays in evaporative saline alkaline lakes can be significant in the formation of abiotic primary dolomite at ambient temperatures as they can generate a gel-like highly viscous medium and provide Mg^{+2} that can enhance the physio-chemical precipitation of primary dolomite from solution. However, more work is needed to better characterize the role of clays for dolomite formation in alkaline lacustrine environments at ambient temperatures.

Acknowledgements

We acknowledge the reviewers, Prof. Armenteros Ildefonso (Geology Department, University of Salamanca, Salamanca, Spain) and Prof. Jose L. Diaz-Hernandez (IFAPA, Área de Recursos Naturales, Consejería de Agricultura, 18080 Granada, Spain) whose suggestions and comments have improved the quality of the manuscript. Dr. W. Haggag (Benha University, Egypt) and Prof. X. Li (School of Earth Sciences and Engineering, Nanjing University, Nanjing, China) are greatly acknowledged for their help during the fieldwork and geochemical analysis. Special thanks are extended to Prof. Jasper Knight (Editor in Chief, Sedimentary Geology) for help in the improvement of the manuscript and editorial support.

References

Abdul Aziz, H., Sanz-Rubio, E., Calvo, J.P., Hilgen, F.J., Krijgsman, W., 2003. Palaeoenvironmental reconstruction of a middle Miocene alluvial fan to cyclic shallow lacustrine depositional system in the Calatayud Basin (NE Spain). Sedimentology 50, 211–236.

Abu El-Ghar, M.S., 2007. Eocene stratigraphy, facies, sequences and depositional history in Shabrawet area, north of Suez, Eastern Desert, Egypt. ISESCO 3, 23–42.

Al-Ahwani, M.M., 1982. Geological and sedimentological studies of Gebel Shabrawet area, Suez Canal district, Egypt. Annals Geological Survey of Egypt 12, 305–379.

Allan, I.R., Wiggins, W.D., 2003. Dolomite Reservoirs: Geochemical Techniques for Evaluating Origin and Distribution. Petroleum Industry Press, Beijing.

Alonso-Zarza, A.M., Bustamante, L., Huerta, P., Rodríguez-Berriguete, A., Huertas, M.J., 2016. Chabazite and dolomite formation in a dolocrete profile: an example of a complex alkaline paragenesis in Lanzarote, Canary Islands. Sedimentary Geology 337, 1–11.

Arenas, C., Casanova, J., Pardo, G., 1997. Stable isotope characterization of the Miocene lacustrine systems of Los Monegros (EbroBasin, Spain): Paleogeographic and paleoclimatatic implications. Palaeogeography. Palaeoclimtology Palaeoecology 128, 133–155.

Arenas, C., Alonso-Zarza, A.M., Pardo, G., 1999. Dedolomitization and other early diagenetic processes in Miocene lacustrine deposits, Ebro Basin (Spain). Sedimentary Geology 125, 23–45.

Armenteros, I., Edwards, N., 2012. Palaeogeographic, palaeoclimatic, palaeohydrological and chemical/biochemical controls on accumulation of late Eocene coastal lacustrine–palustrine limestones, Southern England. Sedimentary Geology 281, 101–118.

Bellanca, A., Calvo, J.P., Censi, P., Neri, R., Pozo, M., 1992. Recognition of lake-level changes in Miocene lacustrine units, Madrid Basin, Spain — evidences from facies analysis, isotope geochemistry and clay mineralogy. Sedimentary Geology 76, 135–153.

Botha, G.A., Hughes, J.C., 1992. Pedogenic palygorskite and dolomite in a Late Neogene sedimentary succession, northwestern Transvaal, South Africa. Geoderma 53, 139–154.

Bréhéret, J.G., Fourmont, A., Macaire, J.J., Négrel, P., 2008. Microbially-mediated carbonates in the Holocene deposits from Sarlièvе, a small ancient lake of the French Massif Central, testify to the evolution of a restricted environment. Sedimentology 55, 557–578.

Brindley, G.W., 1980. Quantitative X-ray analysis of clays. In: Brindley, G.W., Brown, G. (Eds.), Crystal Structures of Clay Minerals and Their X-ray Identification. Mineralogical Society Monograph Vol. 5, pp. 411–438.

Bristow, T.F., Milliken, R.E., 2011. Terrestrial perspective on authigenic clay mineral production in ancient Martian lakes. Clays and Clay Minerals 59, 339–358.

Bristow, T.F., Kennedy, M.J., Morrison, K.D., Mrofka, D.D., 2012. The influence of authigenic clay formation on the mineralogy and stable isotopic record of lacustrine carbonates. Geochimica et Cosmochimica Acta 90, 64–82.

Bustillo, M.A., Alonso-Zarza, A.M., 2007. Overlapping of pedogenesis and meteoric diagenesis in distal alluvial and shallow lacustrine deposits in the Madrid Miocene Basin, Spain. Sedimentary Geology 198, 255–271.

Bustillo, M.A., Arribas, M.E., Bustillo, M., 2002. Dolomitization and silicification in low energy lacustrine carbonates (Paleogene, Madrid Basin, Spain). Sedimentary Geology 151, 107–126.

Calvo, J.P., Jones, B.F., Bustillo, M., Fort, R., Alonso Zarza, A.M., Kendall, C., 1995. Sedimentology and geochemistry of carbonates from lacustrine sequences in the Madrid Basin, central Spain. Chemical Geology 123, 173–191.

Calvo, J.P., Blanc-Valleron, M.M., Rodrigues-Arandia, J.P., Rouchy, J.M., Sanz, M.E., 1999. Authigenic Clay Minerals in Continental Evaporitic Environments. In: Thiry, M., Simon-Coincon, R. (Eds.), Palaeoweathering. Palaeosurfaces and Related Continental Deposits: International Society of Sedimentologists Special Publication Vol. 27, pp. 129–151.

Calvo, J.P., McKenzie, J., Vasconcelos, C., 2003. Microbially mediated lacustrine dolomite formation: evidence and current research trends. In: Valero-Garcés, B.L. (Ed.), Limnogeology in Spain: A Tribute to Kerry Kelts. Consejo Superior de investigaciones Cientificas, Madrid, pp. 229–251.

Casado, A.I., Alonso-Zarza, A.M., Iglesia, A.L., 2014. Morphology and origin of dolomite in paleosols and lacustrine sequences. Examples from the Miocene of the Madrid Basin. Sedimentary Geology 312, 50–62.

Chahi, A., Duplay, J., Lucas, J., 1993. Analyses of palygorskite and associated clays from the Jbel Rhassoul (Morocco): chemical characteristics and origin of formation. Clays and Clay Minerals 41, 401–411.

Chung, F.H., 1974. Quantitative interpretation of X-ray diffraction patterns. I. Matrix-flushing method for quantitative multicompetent analysis. Journal of Applied Crystallography 7, 519–931.

Cuadros, J., Diaz-Hernandez, J.L., Sanchez-Navas, A., Garcia-Casco, A., Jorge Yepes, J., 2016. Chemical and textural controls on the formation of sepiolite, palygorskite and dolomite in volcanic soils. Geoderma 271, 99–114.

Darragi, F., Tardy, Y., 1987. Authigenic trioctahedral smectites controlling pH, alkalinity, silica and Mg-concentration in alkaline lakes. Chemical Geology 63, 457–472.

De Deckker, B.D., Last, M.W., 1989. Modern, non marine dolomite in evaporitic playas of western Victoria, Australia. Sedimentary Geology 64, 223–238.

Deng, S., Dong, H., Lv, G., Jiang, H., Yu, B., Bishop, M.E., 2010. Microbial dolomite precipitation using sulfate reducing and halophilic bacteria: results from Qinghai Lake, Tibetan plateau, NW China. Chemical Geology 274, 151–159.

Deocampo, D.M., 2005. Evaporative evolution of surface waters and the role of crater, northern Tanzania. South African Journal of Geology 108, 493–504.

Deocampo, D.M., 2015. Authigenic clay minerals in lacustrine mudstones. In: Larsen, D., Egenhoff, S.O., Fishman, N.S. (Eds.), Paying Attention to Mudrocks. Geological Society of America, Special Paper Vol. 515, pp. 49–64.

Díaz-Hernández, J.L., Sánchez-Navas, A., Reyes, E., 2013. Isotopic evidence for dolomite formation in soils. Chemical Geology 347, 20–33.

Eberl, D.D., 2003. User guide to RockJock — a program for determining quantitative mineralogy from X-ray diffraction data. United State Geological Society, Open File Report 47, 3–78.

El-Sayed, M., 2001. The nature and possible origin of dolomite in Ar-Rub El-Khali, the UAE. Carbonates and Evaporites 16, 210–223.

Fernández-Díaz, L., Astilleros, J.M., Pina, C.M., 2006. The morphology of calcite crystals grown in a porous medium doped with divalent cations. Chemical Geology 225, 314–321.

Furquim, S.A., Graham, R.C., Barbiero, L., De Queiroz Neto, J.P., Valles, V., 2008. Mineralogy and genesis of smectites in an alkaline-saline environment of Pantanal Wetland, Brazil. Clays and Clay Minerals 56, 579–595.

García del Cura, M.A., Calvo, J.P., Ordóñez, S., Jones, B.F., Cañaveras, J.C., 2001. Petrographic and geochemical evidence for the formation of primary, bacterially induced lacustrine dolomite: La Roda 'white earth' (Pliocene, central Spain). Sedimentology 48, 897–915.

Goldsmith, J.R., Graf, D.L., Heard, H.C., 1961. Lattice constants of the calcium–magnesium carbonates. American Mineralogist 46, 453–457.
Gürel, A., Özcan, S., 2016. Paleosol and dolocrete associated clay mineral occurrences in siliciclastic red sediments of the Late Miocene Kömişini Formation of the Tuzgölü basin in central Turkey. Catena 143, 102–113.
Haggag, W., 2010. Structural Setting an Tectonic Evolution of Gebel Shabrawet Area and Environs, North Eastern Desert, Egypt. Ph.D. Thesis Faculty of Sciences, Benha University (142 pp.).
Hardy, R., Tucker, M., 1988. X-ray powder diffraction of sediments. In: Tucker, M.E. (Ed.), Techniques in Sedimentology. Blackwell Scientific Publications, Oxford, pp. 191–228.
Hassan, M.H., Omran, M.A., 1991. Stratigraphy and depositional history of Shabraweet area, southern Ismailia, Egypt. Middle East Research Centre, Ain Shams University, Earth Science Series 5, 16–30.
Jones, B.F., 1986. Clay mineral diagenesis in lacustrine sediments. In: Mumpton, F.A. (Ed.), Studies in Diagenesis. United State Geological Society Bulletin Vol. 1578, pp. 291–300.
Keyes, M.G., 1925. Making thin sections of rocks. American Journal of Science 10, 538–550.
Koster, M.H., Gilg, H.A., 2015. Pedogenic, palustrine and groundwater dolomite formation in non-marine bentonites (Bavaria, Germany). Clay Minerals 50, 163–183.
Last, W.M., 1990. Lacustrine dolomite: an overview of modern, Holocene and Pleistocene occurrences. Earth-Science Reviews 27, 221–263.
Last, F.M., Last, W.M., Halden, N.M., 2012. Modern and late Holocene dolomite formation: Manito Lake, Saskatchewan, Canada. Sedimentary Geology 281, 222–237.
Leveille, R.J., Longstaffe, F.J., Fyfe, W.S., 2007. An isotopic and geochemical study of carbonate-clay mineralization in basaltic caves: abiotic versus microbial processes. Geobiology 5, 235–249.
Li, X., Xu, W., Liu, W., Zhou, Y., Wang, Y., Sun, Y., Liu, L., 2013. Climatic and environmental indications of carbon and oxygen isotopes from the Lower Cretaceous calcrete and lacustrine carbonates in southeast and Northwest China. Palaeogeography, Palaeoclimatology, Palaeoecology 385, 171–189.
Martín Pérez, A., Alonso Zarza, A.M., La Iglesia, A., Martín García, R., 2015. Do magnesian clays play a role in dolomite formation in alkaline environments? An example from Castañar Cave, Cáceres (Spain). Geogaceta 57, 15–18.
Mauger, C.L., Compton, J.S., 2011. Formation of modern dolomite in hypersaline pans of the Western Cape, South Africa. Sedimentology 58, 1678–1692.
McCrea, J.M., 1950. On the isotopic chemistry of carbonates and a paleotemperatures scale. Journal of Chemical Physics 18, 849–857.
Mercedes-Martin, R., Rogerson, M.R., Brasier, A.T., Vonhof, H.B., Prior, T.J., Fellows, S.M., Reijmer, J.J., Billing, I., Pedley, H.M., 2016. Growing spherulitic calcite grains in saline, hyperalkaline lakes: experimental evaluation of the effects of Mg-clays and organic acids. Sedimentary Geology 335, 93–102.
Morse, J.W., Mackenzie, F.T., 1990. Geochemistry of Sedimentary Carbonates. Developments in Sedimentology 48. Elsevier Science Publishers, the Netherlands 707 pp.
Moustafa, A.R., Khalil, M.H., 1995. Superposed deformation in the northern Suez rift, Egypt: relevance to hydrocarbons exploration. Journal of Petroleum Geology 18, 245–266.
Polyak, V.J., Güven, N., 2000. Authigenesis of trioctahedral smectite in Mg-rich carbonate speleothems in Carlsbad cavern and other caves of the Guadalupe Mountains, New Mexico. Clays and Clay Minerals 48, 317–321.
Pozo, M., Casas, J., 1999. Origin of kerolite and associated Mg clays in palustrine–lacustrine environments. The Esquivias deposit (Neogene Madrid Basin, Spain). Clay Minerals 34, 395–418.
Roberts, J.A., Kenward, P.A., Fowle, D.A., Goldstein, R.H., González, L.A., Moore, D.S., 2013. Surface chemistry allows for abiotic precipitation of dolomite at low temperature. Proceedings of the National Academy of Sciences 110, 14540–14545.
Said, R., 1990. The Geology of Egypt. A.A. Balkema, Rotterdam 734 pp.
Sallam, E., Wanas, H.A., Osman, R., 2015. Stratigraphy, facies analysis and sequence stratigraphy of the Eocene succession in the Shabrawet area (north Eastern Desert, Egypt): an example for a tectonically-influenced inner ramp carbonate platform. Arabian Journal of Geosciences 8, 10433–10458.
Sánchez-Navas, A., Martín-Algarra, A., Rivadeneyra, M.A., Melchor, S., Martín-Ramos, J.D., 2009. Crystal-growth behaviour Ca–Mg carbonate bacterial spherulites. Crystal Growth & Design 9, 2690–2699.
Sánchez-Román, M., Vasconcelos, C., Schmid, T., Dittrich, M., McKenzie, J.A., Zenobi, R., Rivadeneyra, M.A., 2008. Aerobic microbial dolomite at the nanometer scale: implications for the geological record. Geology 36, 879–882.
Selim, S.S., Darwish, M., Abu Khadrah, A.M., 2016. Architecture and evolution of tectonically-induced Middle Eocene clastic wedge on the southern Tethys carbonate shelf. North Eastern Desert, Egypt. Proceedings of the Geologists' Association 127, 377–390.
Sibley, D.F., Gregg, J.M., 1987. Classification of dolomite rock textures. Journal of Sedimentary Petrology 57, 967–975.
Solari, M.A., Hervé, F., Le Roux, J.P., Airo, A., Sial, A.N., 2010. Paleoclimatic significance of lacustrine microbialites: a stable isotope case study of two lakes at Torres del Paine, southern Chile. Palaeogeography, Palaeoclimatology, Palaeoecology 297, 70–82.
Spötl, C., Vennemann, T.W., 2003. Continuous-flow isotope ratio mass spectrometric analysis of carbonate minerals. Rapid Communications in Mass Spectrometry 17, 1004–1006.
Talbot, M.R., 1990. A review of the palaeohydrological interpretation of carbon and oxygen isotopic ratios in primary lacustrine carbonates. Chemical Geology 80, 261–279.
Tosca, N.J., Masterson, A.L., 2014. Chemical controls on incipient Mg-silicate crystallization at 25 °C: implications for early and late diagenesis. Clay Minerals 49, 165–194.
Van Lith, Y., Warthmann, R., Vasconcedos, C., McKenzie, J., 2003. Microbial fossilization in carbonate sediments: a result of the bacterial surface involvement in dolomite precipitation. Sedimentology 50, 237–245.
Vasconcelos, C., McKenzie, J.A., 1997. Microbial mediation of modern dolomite precipitation and diagenesis under anoxic conditions (Lagoa Vermelha, Rio de Janerio, Brazil). Journal of Sedimentary Research 67, 378–390.
Vasconcelos, C., McKenzie, J.A., Bernasconi, S., Grujic, D., Tien, A.J., 1995. Microbial mediation as a possible mechanism for natural dolomite formation at low temperatures. Nature 377, 220–222.
Wacey, D., Wright, D.T., Boyce, A.J., 2007. A stable isotope study of microbial dolomite formation in the Coorong Region, South Australia. Chemical Geology 244, 155–174.
Wanas, H.A., 2002. Petrography, geochemistry and primary origin of spheroidal dolomite from the Upper Cretaceous/Lower Tertiary Maghra El-Bahari Formation at Gabal Ataqa, Northwest Gulf of Suez, Egypt. Sedimentary Geology 151, 211–224.
Wanas, H.A., Sallam, E., Zobaa, M.K., Li, X., 2015. Mid-Eocene alluvial-lacustrine succession at Gebel El-Goza El-Hamra (NE Eastern Desert, Egypt): facies analysis, sequence stratigraphy and paleoclimatic implications. Sedimentary Geology 329, 115–129.
Warren, J., 2000. Dolomite: occurrence, evolution and economically important associations. Earth-Science Reviews 52, 1–81.
Whipkey, Che, E., Hayob, J.L., 2008. Textural and compositional evidence for the evaolution of pedogenic calcite and dolomite in a weathering profile on the Kohala Peninsula, Hawai. Carbonates and Evaporites 23, 104–112.
Whipkey, C.E., Capo, R.C., Hsieh, J.C.C., Chadwick, O.A., 2002. Development of magnesian carbonates in quaternary soils on the island of Hawaii. Journal of Sedimentary Research 72, 158–165.
Wright, D.T., 1999. The role of sulphate-reducing bacteria and cyanobacteria in dolomite formation in the distal ephemeral lakes of the Coorong region, South Australia. Sedimentary Geology 126, 147–157.
Wright, V.P., Barnett, A.J., 2015. An abiotic model for the development of textures in some South Atlantic early Cretaceous lacustrine carbonates. In: Bosence, D.W.J., Gibbons, K.A., le Heron, D.P., Morgan, W.A., Pritchard, T., Vining, B.A. (Eds.), Microbial Carbonates in Space and Time: Implications for Global Exploration and Production. Geological Society of London, Special Publications Vol. 418, pp. 209–219.
Wright, V.P., Wacey, D., 2005. Precipitation of dolomite using sulphate-reducing bacteria from the Coorong Region, South Australia: significance and implications. Sedimentology 52, 987–1008.
Yuan, J., Huang, C., Zhao, F., Pan, X., 2015. Carbon and oxygen isotopic compositions and palaeoenvironmental significance of saline lacustrine dolomite from the Qaidam Basin, Western China. Journal of Petroleum Science and Engineering 135, 596–607.
Zhang, F., Xu, H., Konishi, H., Shelobolina, E.S., Roden, E.E., 2012. Polysaccharide-catalyzed nucleation and growth of disordered dolomite: a potential precursor of sedimentary dolomite. American Mineralogist 97, 556–567.